Confronting a dilaton model with LHC measurements

J. E. Wu[1,*] and Q. S. Yan[2,1,†]

[1]*School of Physics Sciences, University of Chinese Academy of Sciences, Beijing 101408, People's Republic of China*

[2]*Center for Future High Energy Physics, Chinese Academy of Sciences, Beijing 100049, People's Republic of China*

(Received 28 March 2025; accepted 6 March 2026; published 27 March 2026)

The origin of the Higgs boson (H_{125}), discovered in 2012, remains a mystery. In the metric affine theory (MAT) framework, we study the scalar potential and investigate a couple of scenarios for the symmetry breaking mechanisms with a dilaton model which is derived from the geometry. The LHC constraints for the couplings of Yukawa couplings, Higgs-weak vector bosons and Higgs self-couplings, in this model are examined, which identify the parameter space where the discovered Higgs boson $m_h = 125$ GeV can be dilaton-dominant and the features of Higgs self-couplings are explored. It is found that via the measurements of Higgs pair production, the High Luminosity LHC (HL-LHC) running can either confirm or rule out the dilaton dominance.

DOI: 10.1103/ycxz-bvfn

I. INTRODUCTION

Great progress has been achieved recently for the Standard Model (SM) and general relativity (GR), which are both successful theories for interpreting fundamental interactions in nature. The SM has worked quite well in accommodating high-energy data. The Higgs discovery in 2012 is a great leap for the development of particle physics [1,2], which has found the last piece of the SM, H_{125}, and has further confirmed the pillars of the SM, such as the concepts of non-Abelian local gauge theory (Yang-Mills theory), the spontaneous symmetry breaking (SSB), and fermion mass generation via Yukawa type couplings. The GR is applicable to physics on large scales and its prediction is confirmed directly by the first observation of the gravitational wave in 2016 [3]. However, the renormalizability of GR obstructs the quantization of gravity, which is required for the unification of all interactions. Then, it motivates various models to modify gravity [4–6]. Among these models, we are interested in the branch of thoughts which uses scale symmetry to connect the GR with the SM. The localization of the scale symmetry [7–14], which is also called Weyl symmetry or conformal symmetry introduced below, is possible to construct a ultraviolet (UV) complete model.

The concept of gauged scale symmetry was originated from Weyl's work, which was aimed at unifying gravity and electromagnetic theory by introducing a Weyl vector boson to play the role of Maxwell vector field [15]. Due to the fact that it contradicted with the atomic data, the idea was abandoned for a long time. It was revived by Dirac [16] in order to understand the physical laws between cosmological scale and atomic scale. Thus it enlighten a wealth of research for gauge unification theory with the Weyl symmetry [17–20].

The global scale symmetry and its breaking are important guiding principles to formulate its effective Lagrangian and the interaction between the Weyl vector and the Standard Model. The Higgs potential of the SM can be given as

$$V(\phi) = -\mu^2\phi^\dagger\phi + \lambda(\phi^\dagger\phi)^2, \tag{1}$$

where λ is the self-couplings of Higgs boson and μ is a mass parameter which breaks the scale symmetry. The SM preserves the scale symmetry if the parameter $\mu \to 0$. As it is well known that the scale symmetry of fundamental dynamics might related to the dilaton (a singlet field) [21–23], which can be the corresponding Nambu-Goldstone (NG) boson as a massless particle near the electroweak scale. It is natural to conjecture that H_{125} might be related to the dilaton, such as the CFT dilaton [24], the technidilaton (TD) [25], or, more generally, the global scale transformation dilaton [26,27]. However, the gauged scale transformation dilaton has been less discussed.

*Contact author: wujinger22@mails.ucas.ac.cn
†Contact author: yanqishu@ucas.ac.cn

Published by the American Physical Society under the terms of the Creative Commons Attribution 4.0 International license. Further distribution of this work must maintain attribution to the author(s) and the published article's title, journal citation, and DOI. Funded by SCOAP³.

An early attempt which associates Higgs with dilaton giving a gravitational origin for Higgs is shown in [28]. In Ref. [29], the importance of the large nonminimal coupling constant ξ was emphasized and Higgs field was regarded as a physical degree of freedom. Motivated by the great success of gauge theories, Weyl vector was introduced into electroweak (EW) interaction by Cheng [30] through the application of gauged scale symmetry, where the Higgs field was assumed to play the role of Goldstone particle which can be eaten by Weyl vector. In later literature [31,32], one more scalar field was introduced and the Higgs boson can be a physical degree of freedom. The gravitational origin can provide a new perspective on interpreting the SM through an inherent geometry framework [33], which is called Weyl geometry from the prospect of the metric affine theory (MAT) framework [16,34,35].

The referenced studies rely on linear gravity theory, whereas the more natural approach is quadratic gravity within Weyl's geometric framework. Recently a few works [12,14] have applied it to the SM, which is called as the SMW. The SMW is an interesting model which can not only unify the gravity and the SM, but also can have successful inflation, similar to the Starobinsky R^2-inflation. It is curious to us whether the combination of Weyl geometry and SM can accommodate the LHC data, especially the Higgs data, collected over more than a decade [2,36]. To our best knowledge, such a question has not been explored in literature yet. This work is supposed to fill this gap.

In this work, we consider a dilaton model, in which quadratic gravity is embedded in the SM within the Weyl geometry. In the weak eigenstates, there are two scalar fields in the model. The first one is a singlet Φ, which is called as dilaton, and the second one is a doublet ϕ. The H_{125} is parametrized in terms of dilaton and the doublet fields more comprehensively, which yields two different scenarios and can have significantly distinct properties as shown in this work. It is found that our model can accommodate the LHC data, which might be a key to address some BSM issues, such as whether the H_{125} is fundamental or composite, as pointed out by [37–39].

Specifically, the Higgs potentials of the model are confronted with the κ-framework using the latest experimental measurements [40] after spontaneous symmetry breaking of the local scale and electroweak symmetry. We identify the region of parameter space where H_{125} is dilaton-dominant and investigate the capability of the High-Luminosity Large Hadron Collider (HL-LHC) [41] to probe this region. It is found that HL-LHC can confirm/rule out the dilaton dominance.

This paper is organized as given below. In Sec. II, a brief introduction to the dilaton model is given. In Sec. III, two major scenarios of the model are presented. In Sec. IV, a numerical analysis on the parameter space of these two scenarios is provided. In Sec. V, scalar potentials in literature are compared and the electroweak spontaneous symmetry breaking mechanism is examined. Finally, several discussion and conclusions are provided.

II. A BRIEF INTRODUCTION TO THE DILATON MODEL

The similarity of Yang-Mills gauge fields and the affine connections provides a framework to unify the SM and the gravity through the construction of covariant derivative within the perspective of geometry, which can be generalized to the Weyl conformal geometry (indicated by a hat symbol) after extending metricity to the nonmetricity property $\hat{\nabla}_\mu g_{\rho\sigma} = -2\omega_\mu g_{\rho\sigma}$ [34]. The dilaton model includes a singlet real scalar field Φ and a complex doublet scalar for field ϕ, then the nonminimal couplings between scalar fields and Ricci scalar are also included to unify the SM and gravity. The whole Lagrangian can be organized as bosonic and fermionic parts as given below

$$\sqrt{-g}\mathcal{L} = \sqrt{-g}(\mathcal{L}_B + \mathcal{L}_F). \tag{2}$$

where the bosonic part can be written as given below

$$\begin{aligned}
\mathcal{L}_B &= \mathcal{L}_{Bk} + \mathcal{L}_V, \\
\mathcal{L}_{Bk} &= \frac{\hat{R}^2}{4!\xi^2} - \frac{\hat{C}^2_{\mu\nu\rho\sigma}}{\eta^2} - \frac{1}{4g_w^2}\hat{W}^a_{\mu\nu}\hat{W}^{\mu\nu,a} - \frac{1}{4g_s^2}\hat{F}_{\mu\nu}\hat{F}^{\mu\nu} \\
&\quad + \frac{1}{2}\hat{\nabla}_\mu\Phi\hat{\nabla}^\mu\Phi + \hat{\nabla}_\mu\phi^\dagger\hat{\nabla}^\mu\phi, \\
-\mathcal{L}_V &= \frac{\rho}{4!}\Phi^4 + \frac{\alpha}{2}\Phi^2\phi^\dagger\phi + \frac{\lambda}{4}(\phi^\dagger\phi)^2 + \frac{\beta}{2}\Phi^2\hat{R} + \gamma\phi^\dagger\phi\hat{R}.
\end{aligned} \tag{3}$$

In the kinetic terms of the bosonic part, four couplings, ξ, η, g_w, and g_s, are introduced because of the inclusion of the Ricci scalar, the Riemann tensor, the SM gauge bosons, and the Weyl vector. Note that although a relation between $\hat{C}^2_{\mu\nu\rho\sigma}$ and $\hat{F}_{\mu\nu}\hat{F}^{\mu\nu}$ is shown in Eq. (5), both of them are independent and conformally invariant, as discussed in Appendix A of Ref. [19]. In addition to the three free parameters ρ, α, and λ coming from the interactions of the two scalar fields, we have introduced two parameters, β and γ, to describe the nonminimal couplings of the scalar fields to gravity in the potential terms of $\mathcal{L}_V$. In total, there are 9 free parameters. To guarantee that the potential of the system has a bound below, here we assume that $\rho > 0$ and $\lambda > 0$ while α, β, and γ can be either positive or negative.

While the fermionic part can be put as

$$\begin{aligned}\mathcal{L}_F &= \mathcal{L}_{Fk} + \mathcal{L}_Y,\\ \mathcal{L}_{Fk} &= \sum_{g,g'=1,2,3}^{f=q,l}\left(\bar{\Psi}_L^{gf}\hat{\not{D}}\Psi_L^{gf} + \bar{\Psi}_{1R}^{gq}\hat{\not{D}}\Psi_{1R}^{gq} + \bar{\Psi}_{2R}^{gf}\hat{\not{D}}\Psi_{2R}^{gf}\right)\\ &\quad + \cdots\\ -\mathcal{L}_Y &= \sum_{g,g'=1,2,3}^{f=q,l}\left(Y_{gg'}^{q}\bar{\Psi}_L^{\prime gq}\tilde{\phi}\Psi_{1R}^{g'q} + Y_{gg'}^{f}\bar{\Psi}_L^{gf}\phi\Psi_{2R}^{g'f}\right)\\ &\quad + \ldots + \text{H.c.},\end{aligned} \tag{4}$$

where the fermion fields Ψ_L^{gf} for the left-handed $SU(2)$ doublet and Ψ_{iR}^{gf} for the right-handed $SU(2)$ singlet are introduced. The index $i = 1, 2$ corresponds to the upper and lower components of the doublet, where f denotes the fermion type (such as quarks q or leptons l), and g (or g') labels the fermion generations. Here only the fermionic part of the SM is presented. New physics can be introduced by including new fermions and their new interactions with the dilaton Φ, as denoted by $\cdots$ in both fermionic kinetic and Yukawa terms.

The squared Weyl tensor $\hat{C}^2_{\mu\nu\rho\sigma}$, the Weyl scalar curvature $\hat{R}$ and the derivative $\hat{\nabla}_\mu$ of the scalar can be further expressed as the quantities of Riemannian geometry with the Weyl vector ω_μ.

$$\begin{aligned}\hat{C}^2_{\mu\nu\rho\sigma} &= C^2_{\mu\nu\rho\sigma} + 6F_{\mu\nu}F^{\mu\nu},\\ \hat{R} &= R - 6(\omega_\mu\omega^\mu + \nabla_\mu\omega^\mu),\\ \hat{\nabla}_\mu\phi &= \nabla_\mu\phi + d_\phi\omega_\mu\phi = \nabla_\mu\phi - \omega_\mu\phi,\end{aligned} \tag{5}$$

where ∇_μ is Riemannian derivative and the Weyl weight $d_\phi = -1$ is given by the transformation in Eq. (6). $C_{\mu\nu\rho\sigma}$ is the traceless part of Riemannian curvature tensor $R_{\mu\nu\rho\sigma}$, known as Riemannian Weyl tensor. Ricci scalar is defined as $R = g^{\mu\nu}R_{\mu\nu}$, the second-rank Ricci tensor is defined as $R_{\mu\nu} = R^\alpha_{\mu\alpha\nu}$ and the four-rank Riccis tensor is defined as $R^\alpha_{\beta\mu\nu} = \partial_\mu\Gamma^\alpha_{\beta\nu} - \partial_\nu\Gamma^\alpha_{\beta\mu} + \Gamma^\alpha_{\gamma\mu}\Gamma^\gamma_{\beta\nu} - \Gamma^\alpha_{\gamma\nu}\Gamma^\gamma_{\beta\mu}$, which are connected with the Euler-Gauss-Bonnet term [42,43] showing the completeness of Eq. (3). All of them are dependent upon the metric $g_{\mu\nu}$ which satisfies the metric compatibility and the Levi-Civita connection $\Gamma^\rho_{\mu\nu}$ which is defined as $\Gamma^\rho_{\mu\nu} = \frac{1}{2}g^{\rho\alpha}(\partial_\mu g_{\nu\alpha} + \partial_\nu g_{\mu\alpha} - \partial_\alpha g_{\mu\nu})$.

The antisymmetric tensor $\hat{F}_{\mu\nu}$ is related to the Weyl vector field ω_μ, and is defined as $\hat{F}_{\mu\nu} = F_{\mu\nu}$ because of torsionless. Thus, the tensor $F_{\mu\nu}$ can be simplified as $F_{\mu\nu} = \partial_\mu\omega_\nu - \partial_\nu\omega_\mu$. And W^a_μ denotes the gauge fields (weak and hypercharged vector fields) of the SM.

The Lagrangian is constructed based on local gauge symmetries, encompassing not only the SM but also the scale transformation in the following equation (6), which is natural to consider within the Weyl geometry.

$$\begin{aligned} g_{\mu\nu} &\to \Omega^2 g_{\mu\nu}, & g^{\mu\nu} &\to \Omega^{-2}g^{\mu\nu},\\ \hat{R} &\to \Omega^{-2}\hat{R}, & \hat{C}_{\mu\nu\rho\sigma} &\to \Omega^{-2}\hat{C}_{\mu\nu\rho\sigma},\\ \Phi &\to \Omega^{-1}\Phi, & \varphi &\to \Omega^{-1}\varphi,\\ \Psi &\to \Omega^{-3/2}\Psi, & \omega_\mu &\to \omega_\mu - \partial_\mu\ln\Omega,\end{aligned} \tag{6}$$

Such a local gauged Weyl conformal transformation is also called as $D(1)$ symmetry, which is an Abelian type symmetry as demonstrated from this definition. It is noteworthy that the local gauge fields of the SM W^a_μ are invariant under such a transformation.

This local gauged conformal symmetry must be broken at some energy scale. In literature, there are three methods of conformal symmetry breaking.

(i) The first one is Coleman-Weinberg mechanism [44]. Although the potential remains invariant under conformal transformations at tree level, the inclusion of quantum corrections to the Lagrangian breaks this conformal symmetry through dimensional transmutation.

(ii) The second method is to introduce some terms with dimensional parameters, which explicitly break the conformal symmetry [45].

(iii) The third one is Stueckelberg mechanism, where without knowing how the conformal symmetry is broken dynamically, a pseudo-Nambu-Goldstone particle can be introduced. The Weyl vector field becomes massive after eating the this Goldstone field [11,30,46].

In this work, we adopt the third method to elucidate the spontaneous breaking of conformal symmetry. This breaking generates a nonvanishing mass term for the scalar field, which provides a seed for the spontaneous symmetry breaking of EW gauge symmetry in the SM.

Notice that the scalar-tensor Lagrangian given in Eq. (3) is quadratic, which is a good candidate for quantum gravity. However, in order to return back to the GR, we can define a Brans-Dicke (BD) field Θ to linearize the Lagrangian since all quadratic theory, or more generally, for modified f(R) theory, can be linearized as a BD type theory [47]

$$\Theta^2 \coloneqq \chi'^2_D\Phi^2 + \chi'^2_H H^2, \tag{7}$$

where $H^2 = 2\phi^\dagger\phi$ denotes the modulus of the complex doublet. When the dilaton and doublet acquire vacuum expectation values (VEVs), the Brans-Dicke field also develops a VEV f causing the breaking of the local conformal symmetry.

Apparently, there could exist three different energy scales in the model. One scale is f_D, i.e., the VEV of Φ. The other is f_H, the VEV of ϕ. The third scale is f, which can be related to f_D and f_H via the following relation

$$f^2 = \chi'^2_D f_D^2 + \chi'^2_H f_H^2 \tag{8}$$

Due to the nonminimal coupling, f^2 could be related to the scale of gravity, i.e., Λ_{Planck}, though it is not necessarily. Obviously, either f_D or f_H or both, can trigger the conformal symmetry breaking.

Meanwhile, it should be pointed out that the parameters χ'^2_D and χ'^2_H are not necessarily $O(1)$, i.e., they might be large or huge numbers, saying 10^{36} if we want to generate the Planck energy scale from the electroweak scale, which is taken as 246 GeV, as demonstrated in [30]. When f is assumed to be around $\sim\Lambda_{\text{Planck}}$, the model can be an inflaton model as investigated by Ref. [12].

After the conformal symmetry breaking, we can parametrize Θ^2 as

$$\Theta^2 \coloneqq f^2\Sigma^2, \tag{9}$$

with $\Sigma^2 = \Theta^2/\langle\Theta^2\rangle = \Theta^2/f^2$, which is a dimensionless field. From Eq. (3), parameters χ'^2_D (χ'^2_H) can be found which include β (γ) and also ξ^2 due to the linearization of the quadratic effect. In literature, the field Σ can be parametrized in a nonlinear form as

$$\Sigma \coloneqq \exp\left[\frac{d}{f}\right], \tag{10}$$

In this parametrization, Σ plays the role of Goldstone boson and it can be eaten by the Weyl vector boson which becomes massive.

There is one point worthy of stress. A conformal coupling constant $\frac{D-2}{4(D-1)}$ is typically required for a D-dimensional nonminimal coupling scalar theory [48]. Thus, it seems that there should be a constraint on the free parameters of our model. However, it turns out this is not a constraint. Before the local scaling symmetry breaking, due to Weyl's geometry, the local conformal symmetry is preserved and it is observed that the factor **6** in the second equation of (5) aligns with the conformal coupling constant. Therefore, there is no constraint on β and γ. After the local conformal symmetry being broken, typically the nonminimal coupling between BD scalar and R can be parametrized as ω, which is assumed to be a free parameter, as a common practice for BD theory [49].

By using the following gauge fixing conditions (unitary gauge)

$$\bar{g}_{\mu\nu} = \Sigma^2 g_{\mu\nu}, \qquad \bar{\omega}_\mu = \omega_\mu - \partial_\mu \ln\Sigma, \tag{11}$$

where $\bar{g}_{\mu\nu}$ and $\bar{\omega}_\mu$ are physical fields, we can eliminate the Goldstone of conformal symmetry breaking from the Lagrangian.

Here it is helpful to count the degrees of freedom of the model before and after Θ develops VEV. Before the symmetry breaking, there are four degrees of freedom in ϕ and one in Φ, i.e. Θ includes a combination of 5 degrees of freedom. Below we can consider two cases where the symmetry breaking is driven dominantly either by the dilaton Φ or by the doublet ϕ.

(i) In the first case where the symmetry breaking is dominantly driven by the dilaton Φ, $f^2 \approx \chi_D^2 f_D^2$, and the Goldstone d is from Φ. After taking unitary gauge, at the low energy region, only doublet ϕ is left and a mass term is generated. After ϕ develops VEV, the electroweak symmetry $SU(2)_L \times U_Y(1)$ is broken, and after taking unitary gauge for weak gauge bosons, only one degree of freedom is left, which corresponds to H_{125}.

(ii) In the second case where the symmetry breaking is dominantly driven by the doublet ϕ, $f^2 \approx \chi_H^2 f_H^2$, and the Goldstone d is from the doublet ϕ. After taking unitary gauge for Weyl vector and weak vector gauge fields, at the low energy region, only the dilaton Φ is left. After Φ develops VEV, the $D(1)$ symmetry is broken, only one degree of freedom is left, which is the H_{125}. If this case is the reality, it is an issue how this singlet couples to the SM fermions. Thus new physics must be needed in order to cure this issue.

III. TWO SCENARIOS OF THE MODEL

After BD filed Θ develops its VEV, there exist two possible parametrizations. One is

$$\Theta^2 = f^2\Sigma^2 = f^2\Sigma^2\sin^2\theta + f^2\Sigma^2\cos^2\theta, \tag{12}$$

and the other is

$$\Theta^2 = f^2\Sigma^2 = f^2\Sigma^2\cosh^2\theta - f^2\Sigma^2\sinh^2\theta, \tag{13}$$

where θ is an angle which represents the degree of freedom left in the low energy region. Which form of Θ^2 should be taken depends upon the relative signs of χ_D^2 and χ_H^2.

Below we systematically analyse the scenarios in term of the relative signs of χ'^2_D and χ'^2_H.

Although the specific form of $\chi'_{H,D}$ depends on the linearization, Eq. (3) gives $\chi'^2_D = \beta + k_D$ and $\chi'^2_H = \gamma + k_H$, where $k_{D/H}$ represent functions designed to linearize the quadratic curvature term. Since the signs of β and γ are not specified, the signs of χ'^2_D and χ'^2_H remain undetermined, resulting in four possible scenarios. (1) the first trigonometric scalar scenario (TSS1) with $\chi'^2_D > 0$ and $\chi'^2_H > 0$, (2) the second trigonometric scalar scenario (TSS2) with $\chi'^2_D < 0$ and $\chi'^2_H < 0$, (3) the frist hyperbolic scalar scenario (HSS1) with $\chi'^2_D > 0$ and $\chi'^2_H < 0$, and (4) the second hyperbolic scalar scenario (HSS2) with $\chi'^2_D < 0$ and $\chi'^2_H > 0$, as tabulated in Table I. Owing to the reason that the TSS2 cannot produce the correct sign in the GR, we will not consider it here. Thus, we can label TSS1 as TSS for simplicity. Also it should be noticed that the parametrization is democratic for either the real scalar

TABLE I. The definitions of scenarios are tabulated.

Scenarios	$\chi'^2_D > 0$	$\chi'^2_D < 0$
$\chi'^2_H > 0$	TSS1	HSS2
$\chi'^2_H < 0$	HSS1	TSS2

and the complex doublet, which means the similarity for HSS1 and HSS2. Therefore, we can just consider HSS1 without losing generality and define it as HSS in the discussion below.

In the TSS, we can parametrize doublet and dilaton scalar fields by $\chi_H^2 = \chi'^2_H > 0$ and $\chi_D^2 = \chi'^2_D > 0$ into the following form

$$H^2 = \frac{f^2}{\chi_H^2}\Sigma^2 \sin^2\theta, \qquad \Phi^2 = \frac{f^2}{\chi_D^2}\Sigma^2\cos^2\theta. \tag{14}$$

Substituting complex and dilaton fields into the Lagrangian and using the unitary gauge given in Eq. (11), we can arrive at a Lagrangian with only physical fields.

The Higgs potential can be computed as given below

$$\begin{aligned} V &= \frac{f^4\rho}{4!\chi_D^4} - \frac{T_t^2}{2}\frac{f^2}{\chi_H^2}\sin^2\left[\frac{\chi_H}{f}\theta'\right] + \frac{F_t}{4}\frac{f^4}{\chi_H^4}\sin^4\left[\frac{\chi_H}{f}\theta'\right], \\ &\approx \frac{f^4\rho}{4!\chi_D^4} - \frac{F_t U_t^4}{4} + T_t^2(1-s^2)h^2 + F_t U_t\sqrt{1-s^2}(1-2s^2)h^3 \\ &\quad - \frac{F_t}{4}\left(1 - \frac{28s^2}{3}(1-s^2)\right)h^4 + \ldots. \end{aligned} \tag{15}$$

where the $\cdots$ denote high order terms, like h^6 and h^8 or higher terms. In order to cast the Higgs potential into the standard form, some shorthanded parameters are defined and given below

$$\begin{aligned} &T_t^2 = \frac{f^2}{2\chi_D^2}\left(\frac{\rho\chi_H^2}{3\chi_D^2} - \alpha\right) > 0, \\ &F_t = \lambda + \frac{\rho\chi_H^4}{6\chi_D^4} - \frac{\alpha\chi_H^2}{\chi_D^2} > 0, \qquad U_t \coloneqq \sqrt{\frac{T_t^2}{F_t}}, \\ &\theta' = \frac{f}{\chi_H}\theta \coloneqq f_{\mathrm{EW}} + h, \qquad f_{\mathrm{EW}} = \frac{f}{\chi_H}\arcsin\left[\frac{\chi_H}{f}U_t\right]. \end{aligned} \tag{16}$$

The full form of the Higgs potential of TSS is shown as the first line, which is periodic due to the periodicity of the trigonometric functions. While the form in the second line is obtained by using Taylor expansion. It should be pointed out that the expansion is based on $\sin[\frac{\chi_H}{f}h]$, not on $\sin[\frac{\chi_H}{f}\theta']$ instead. Here h denotes H_{125} and the parameter U_t is the VEV of the trigonometric scenario of the electroweak scalar $\sin[\frac{\chi_H}{f}\theta]$ in our model.

The BSM deviations of Higgs couplings are described using the κ-framework, and by analogy, we also define the deviations in the VEV[1] and the masses of the W boson and the Higgs boson which are listed with all relevant κ parameters in Table II.

TABLE II. The κ parameters in TSS are listed.

κ	TSS
κ_v	$\frac{U_t}{v}\arcsin[s]/s$
κ_{m_W}	$\kappa_v\sqrt{1-\chi s^2}$
κ_{m_h}	$\frac{T_t}{\mu}\sqrt{1-s^2}$
κ_V	$\kappa_v\left[1-\chi s\left(\sqrt{1-s^2}\arcsin[s]+s\right)\right]$
κ_f	$\frac{1}{\kappa_{m_W}}\frac{\arcsin s}{s}\sqrt{(1-s^2)(1-\chi s^2)}$
κ_{2V}	$1-\chi[\arcsin^2[s](1-2s^2)+4\arcsin[s]s\sqrt{1-s^2}+s^2]$
κ_{3h}	$\frac{F_t U_t}{\lambda_{\mathrm{SM}} v}(1-2s^2)\sqrt{1-s^2}$
κ_{4h}	$\frac{F_t}{\lambda_{\mathrm{SM}}}(1-\frac{28}{3}s^2(1-s^2))$

It should be pointed out that these κ parameters are characterized by two parameters, i.e., χ and s, which are defined as given below

$$\begin{aligned} &\chi \coloneqq 1 - \frac{\chi_H^2}{\chi_D^2} < 1, \\ &s \coloneqq= \frac{\chi_H U_t}{f} = \sin\left[\frac{\chi_H}{f}f_{\mathrm{EW}}\right] > 0, \end{aligned} \tag{17}$$

where the parameter χ measures the discrepancy of scalars, it is 1 when $\chi_H^2 \to 0$ and zero when $\chi_H^2 = \chi_D^2$. While the parameter s measures the scale symmetry breaking caused by the doublet ϕ, and it is 0 when $\chi_H \to 0$ and 1 when $\chi_H U_t \to f$. It is symmetric for $s > 0$ and $s < 0$ due to a Z_2 symmetry of Higgs potential. For the sake of simplicity, we will focus on the case where $s > 0$.

For the HSS, scalar fields can be parametrized using $\chi_H^2 = -\chi'^2_H > 0$ and $\chi_D^2 = \chi'^2_D > 0$ as follows

$$H^2 = \frac{f^2}{\chi_H^2}\Sigma^2\sinh^2\theta, \qquad \Phi^2 = \frac{f^2}{\chi_D^2}\Sigma^2\cosh^2\theta. \tag{18}$$

Substituting these parametrization and using the unitarity gauge to the Lagrangian, the corresponding Higgs potential can be obtained

[1]Notice that $\kappa_v = \frac{f_{\mathrm{EW}}}{v}$ does not need to equal 1 because f_{EW} is defined before canonicalization.

TABLE III. The κ parameters in the HSS are tabulated.

κ	HSS
κ_v	$\frac{U_h}{v}\text{arcsinh}[s]/s$
κ_{m_W}	$\kappa_v\sqrt{1+\chi s^2}$
κ_{m_h}	$\frac{T_h}{\mu}\sqrt{1+s^2}$
κ_V	$\kappa_v\left[1+\chi s\left(\sqrt{1+s^2}\text{arcsinh}[s]+s\right)\right]$
κ_f	$\frac{1}{\kappa_{m_W}}\frac{\text{arcsinh}s}{s}\sqrt{(1+s^2)(1+\chi s^2)}$
κ_{2V}	$1+\chi\left[\text{arcsinh}^2[s](1+2s^2)+4\text{arcsinh}[s]s\sqrt{1+s^2}+s^2\right]$
κ_{3h}	$\frac{F_h U_h}{\lambda_{\rm SM} v}(1+2s^2)\sqrt{1+s^2}$
κ_{4h}	$\frac{F_h}{\lambda_{\rm SM}}[1+\frac{28}{3}s^2(1+s^2)]$

$$V=\frac{f^4\rho}{4!\chi_D^4}-\frac{T_h^2 f^2}{2\chi_H^2}\sinh^2\left[\frac{\chi_H}{f}\theta'\right]+\frac{F_h f^4}{4\chi_H^4}\sinh^4\left[\frac{\chi_H}{f}\theta'\right],$$
$$\approx\frac{f^4\rho}{4!\chi_D^4}-\frac{F_h U_h^4}{4}+T_h^2(1+s^2)h^2+F_h U_h\sqrt{1+s^2}(1+2s^2)h^3$$
$$+\frac{F_h}{4}\left(1+\frac{28s^2}{3}(1+s^2)\right)h^4+\ldots, \quad (19)$$

with the following parameters being defined

$$T_h^2=-\frac{f^2}{2\chi_D^2}\left(\alpha+\frac{\rho\chi_H^2}{3\chi_D^2}\right)>0,$$
$$F_h=\lambda+\alpha\frac{\chi_H^2}{\chi_D^2}+\frac{\rho\chi_H^4}{6\chi_D^4}>0, \quad U_h\coloneqq\sqrt{\frac{T_h^2}{F_h}},$$
$$\theta'=\frac{f}{\chi_H}\theta\coloneqq f_{\rm EW}+h, \quad f_{\rm EW}=\frac{f}{\chi_H}\text{arcsinh}\left[\frac{\chi_H}{f}U_h\right]. \quad (20)$$

Obviously, the potential of HSS possesses no periodicity, in contrast to that of the TSS. The potential can be expanded by using the Taylor expansion in term of $\sinh[\frac{\chi_H}{f}h]$ rather than $\sinh[\frac{\chi_H}{f}\theta']$, which is given in the second line. One should realize that the difference for these two scenarios lies in the difference of trigonometric and hyperbolic functions.

From the Lagrangian, we extract the κ values and present them for the HSS in Table III which are dependent upon two parameters χ and s being defined below

$$\chi\coloneqq 1+\frac{\chi_H^2}{\chi_D^2}>1,$$
$$s\coloneqq\frac{\chi_H U_h}{f}=\sinh\left[\frac{\chi_H}{f}f_{\rm EW}\right]>0. \quad (21)$$

IV. NUMERICAL ANALYSIS ON THE DILATON DOMINANCE

We adopt two analysis methods: one is a global fitting (GF) method, the other is specific solution (SS) method. Below we examine these two scenarios by using the LHC experimental measurements presented in Table IV. After taking into account the requirement of Eqs. (17)–(21), the allowed parameter space in the $\chi-s$ plane determined by these two methods can be found for these two scenarios in Figs. 1 and 2.

To examine the effects of Yukawa couplings, we present the global fitting results with all data (including κ_f measurements) given in Table IV and the fitting results without κ_f measurements. We consider a fit with 4 free parameters, i.e., s, χ, T, and F, by using the relations in Tables II and III. When the results are projected on the $s-\chi$ plane, for the TSS scenario, the best-fit values from all measurements (without κ_f data) are given as $s=0.07(0.04)$ and $\chi=-7.46(-10.65)$, with the $\chi^2_{\rm min}=1.93(0.65)$; While for the HSS scenario, the best-fit values are given as $s=4.16(3.50)\times10^{-5}$ and $\chi=1.14(1.15)$, with $\chi^2_{\rm min}=1.94(0.84)$ indicated by the five-angle star in the figure. All fits are considered good since their p-values exceed 50%. The global fitting results indicate that the model can accommodate the experimental data quite well.

From our results, it is also clear that in essential, our global fitting demonstrates that the SM is favored by the experimental data, which corresponds to the limit $s\to0$ and is represented by the purple line in each of these two figures.

The 2σ contours of the fits are shown, with the color shaded region bounded by a dot-dashed line corresponding to the results using only bosonic processes without the κ_f data, whereas the color shaded region bounded by a thick solid line corresponds to the results including all LHC measurements.

TABLE IV. The values of κ from LHC measurements are provided.

κ_{m_W}	$1.00014^{+0.00021}_{-0.00021}$ (99.98% CL) [50]
κ_{m_h}	$1.00176^{+0.001118}_{-0.001118}$ (99.89% CL) [51]
κ_V	$1.035^{+0.077}_{-0.074}$ (95% CL) [52]
κ_t	$0.99^{+0.09}_{-0.08}$ (90% CL) [53]
κ_b	$0.90^{+0.12}_{-0.11}$ (90% CL) [53]
κ_τ	$0.95^{+0.10}_{-0.08}$ (90% CL) [53]
κ_μ	$1.05^{+0.25}_{-0.31}$ (90% CL) [53]
κ_{2V}	$0.92^{+0.58}_{-1.52}$ (95% CL) [40]
κ_{3h}	$4.3^{+2.9}_{-5.5}$ (95% CL) [40]

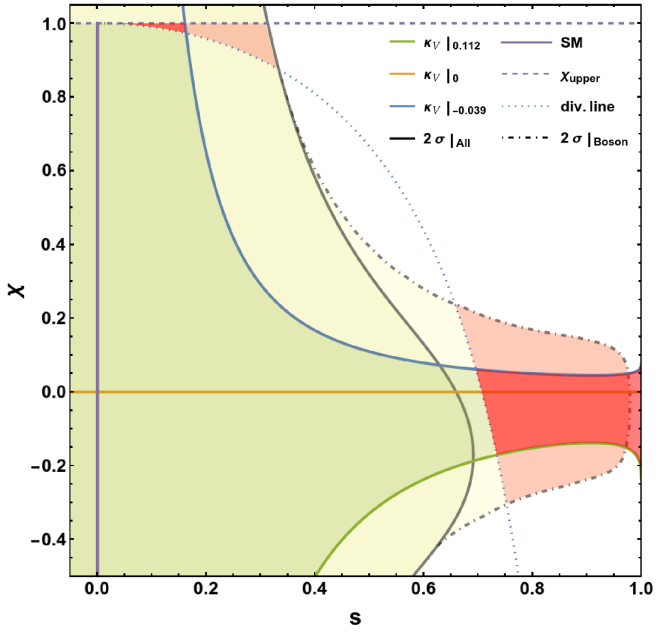


FIG. 1. Allowed parameter space by experiments for TSS in χ and s plane is shown.

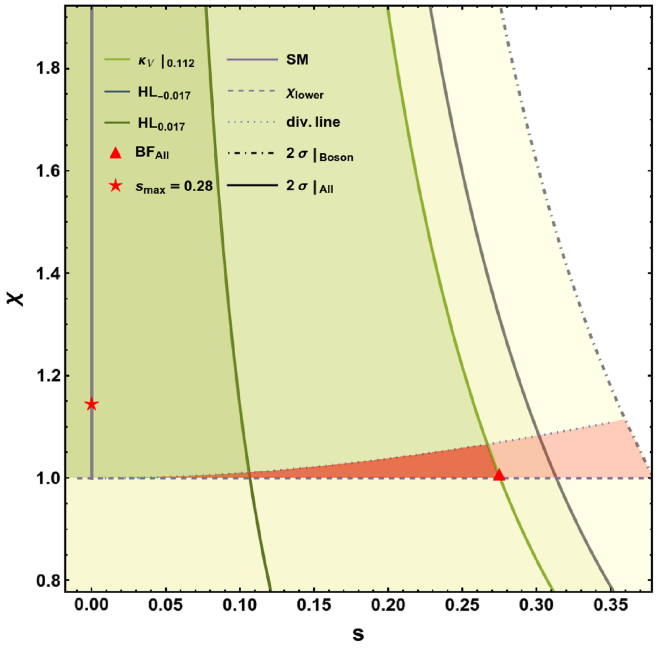


FIG. 2. Allowed parameter space in the HSS is shown.

According to the definitions in Eqs. (14) and (18), the dividing line of doublet-dominant or dilaton-dominant is determined by Eq. (22)

$$\left.\frac{\Phi^2}{H^2}\right|_{\rm TSS} \to \left.\frac{\chi_H^2}{\chi_D^2}\frac{\cos[\frac{\chi_H}{f}\theta]}{\sin[\frac{\chi_H}{f}\theta]}\right|_{\rm vev} = (1-\chi)\frac{1-s^2}{s^2} = 1,$$
$$\left.\frac{\Phi^2}{H^2}\right|_{\rm HSS} \to \left.\frac{\chi_H^2}{\chi_D^2}\frac{\cosh[\frac{\chi_H}{f}\theta]}{\sinh[\frac{\chi_H}{f}\theta]}\right|_{\rm vev} = (\chi-1)\frac{1+s^2}{s^2} = 1, \qquad (22)$$

and the parameter regions where the ratio is smaller (larger) than 1 is defined as dilaton (doublet) dominance. These two parameter regions is separated by the dotted line in these figures, while the doublet-dominant region is shaded in blue and the dilaton-dominant region is shaded in red.

Apart from the GF method, we also perform a detailed analysis by using the SS method, in which we use the mass of the W boson [54], the mass of the Higgs boson [55], and the coupling κ_V [52] as model inputs to solve out the border of allowed parameter space. In practice, we fix $\kappa_{m_W} = 1$, and $\kappa_V = 1 + \delta$ (95% CL) is taken from the experimental results reported in [52]

$$\kappa_V = 1.035^{+0.077}_{-0.074} = 1^{+0.112}_{-0.039}. \qquad (23)$$

The projected precision of HL-LHC $\kappa_V = 1 \pm 0.017$ (68% CL) [41] are also illustrated as darker lines and shaded region in Fig. 2.

In the SS method, the measurements of Yukawa couplings require $\kappa_f = 0.979^{+0.114}_{-0.105}$(95% CL) [53] which constrain the model parameters, like s, as shown in Fig. 3 by the yellow shaded region in the $\kappa_f - s$ plane. The upper and lower panels of this figure correspond to the TSS and HSS scenarios, respectively. It is obtained by assuming $\kappa_{m_W} = 1$, with the fermion masses fixed to their SM values, and the red shaded region denotes the parameter space of dilaton dominance (the legend is the same as in Fig. 1 and Fig. 2).

As illustrated in Fig. 3, the dilaton-dominant interpretation still exists, although a larger fraction of parameter space favors the doublet-dominant interpretation of H_{125}. Such a conclusion also hold when all Higgs data are taken

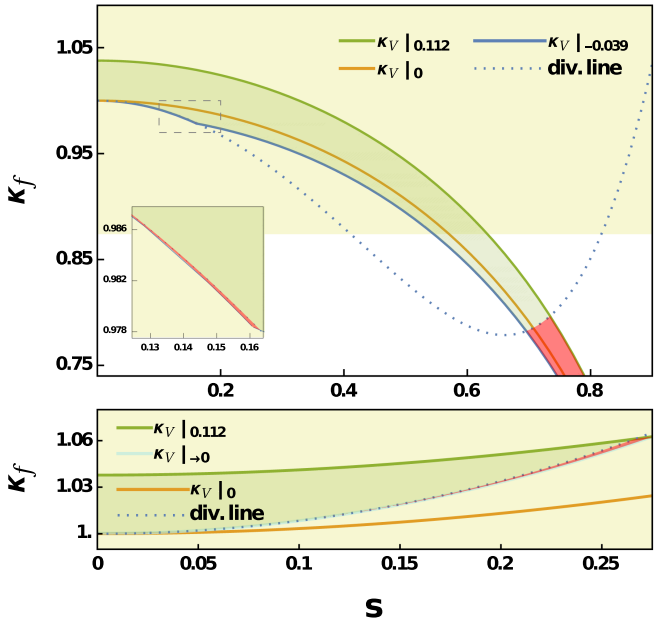


FIG. 3. The constraints on κ_f in the TSS(upper)/HSS(lower) scenarios are shown.

into account and is consistent with the global fitting results given in Figs. 1 and Fig. 2.

In the HSS scenario, the entire dilaton-dominant region lies within the 95% CL of the experimental constraint on κ_f, as shown in Fig. 2 and the lower panel plot of Fig. 3. In contrast, in the TSS scenario, there are two separate regions for the dilaton dominance, one is outside the 95% CL for $s > 0.6$, the other is for $s < 0.2$, as illustrated in the closeup inset in the upper panel plot of Figs. 3 and 1. The enlarged inset in the upper panel plot of Fig. 3 highlights the viable region in the $s \to 0$, $\chi \to 1$ regime shown in Fig. 1, corresponding to the limit $\chi_H \to 0$ where $f^2 \approx \chi_H^2 f_H^2$ given $f_H \gg f_D$. This parameter region is narrow but is still allowed, which could be ruled out only if the HL-LHC measurement would exclude the case $\kappa_V < 1$.

After examining the effects of Yukawa couplings, below we also examine the prediction of Higgs-weak boson couplings and Higgs self couplings of the model in the SS method. When we fix $\kappa_{m_h} = 1$, the predicted Higgs trilinear couplings can be determined as

$$\kappa_{3h} = \frac{FU}{\lambda_{\rm SM} v}(1-2s^2)\sqrt{1-s^2}, \xrightarrow{\kappa_{m_h}=1} \frac{\mu^2}{\lambda_{\rm SM} v^2}\frac{\arcsin[s]}{s\sqrt{1-s^2}}(1-2s^2)\sqrt{1-\chi s^2}. \quad (24)$$

In particular, for TSS, we focus on the analysis of the solution $\chi = 0$, since it can lead an interesting relation $\chi_D^2 = \chi_H^2$. Consequently, the couplings between the Weyl vector and Higgs are decoupled, and $\kappa_{2V} = 1$ in TSS. More discussion of the couplings to fermions can be found in Ref. [12].

The relationships between κ_{3h}, κ_{4h}, and s are depicted by the orange and darker orange lines, respectively, in Fig. 4. The experimental measurements of κ_{3h} from Table IV are depicted as the lighter blue shaded region, constraining $s < 0.87$. Meanwhile, the projected precision of the HL-LHC [41] at 68% CL for $0.52 < \kappa_\lambda < 1.50$ is also shown by the darker blue shaded region.

The four-pointed star marker separates the allowed parameter of s into two parts. The first part is $0 < s < \frac{1}{\sqrt{2}}$, where the scalar H_{125} corresponds to doublet dominance since H_{125} is mainly from complex doublet. While the second part is $\frac{1}{\sqrt{2}} < s \leq 0.87$, where the scalar H_{125} is dilaton boson dominant from scalar singlet mainly. Notice that $s = \frac{1}{\sqrt{2}}$ is the maximum mixture sate for the doublet and dilaton, making it difficult to distinguish whether the doublet or dilaton dominates. Furthermore, it is observed that the HL-LHC run is capable to confirm/rule out the parameter space of dilaton dominance.

The dilaton-dominant region, defined by $\frac{1}{\sqrt{2}} \leq s \leq 0.87$, predicts a negative Higgs self-coupling for both three-point and four-point interactions. It is remarkable that even for the doublet-dominant region $0 \leq s \leq \frac{1}{\sqrt{2}}$, the quartic Higgs self-coupling can be either positive or negative, and a vanishing quartic coupling is also possible. This distinctive feature originates from the TSS scenario, resulting in a periodic potential.

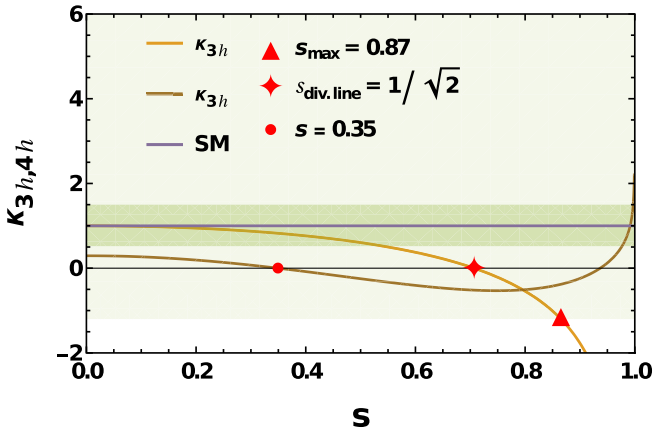


FIG. 4. The varying of $\kappa_{3h/4h}$ with parameter s in the TSS are shown($\chi = 0$).

For a potential of ϕ^4 theory, a negative quartic coupling means that the vacuum is unstable. In the SM, a negative quartic coupling of Higgs potential means the potential is unbounded below [56]. However, it should be pointed out that the vacuum stability in the TSS of our model is ensured, as demonstrated by the full form of the potential given in Eq. (15). In the form of its Taylor expansion, there are higher order terms like h^6 and h^8, etc., which can guarantee the vacuum stability of our model.

Since s is tightly constrained by the upper bound on κ_V (as illustrated in Fig. 2), our analysis emphasizes this constraint in Fig. 5. The triangular marker line indicates the maximum value of s, while the four-point marker line marks the demarcation between doublet- and dilaton-dominant regions along the allowed blue curve. The quantities κ_{2V}, κ_{3h}, and κ_{4h}, which depend on the upper bound of κ_V and vary with s, are depicted by the light blue, blue, and darker blue lines, respectively. It is obvious that

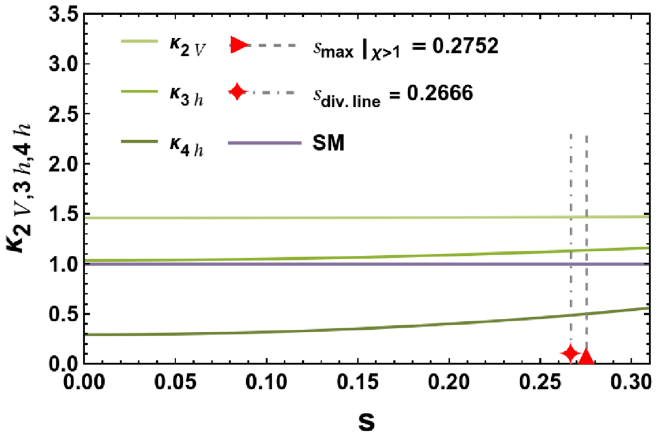


FIG. 5. The constraints to $\kappa_{2V/3h/4h}$ in the HSS are shown.

these measurements are not sensitive to the breaking of scale symmetry s in HSS, which will be difficult to be measured even at the future 100 TeV colliders [57–59]. Nonetheless, the measurements can be enhanced due to the sensitivity of κ_V, with improved precision provided by the HL-LHC, as shown in Fig. 2 introduced above.

V. SCALARS POTENTIALS AND SPONTANEOUS SYMMETRY BREAKING

In Table VI, we also list a few typical scalar potentials in literatures which can trigger spontaneous symmetry breaking and compare the shapes of these potentials in Fig. 6.

In the Ref. [12], the Higgs potential in the SMW is found to have the following form

$$V(\sigma)=\frac{3}{2}M_p^2\left[6\lambda\sinh^4\frac{\sigma}{M_p\sqrt{6}}+\xi^2\left(1-\xi_h\sinh^2\frac{\sigma}{M_p\sqrt{6}}\right)^2\right], \tag{25}$$

where σ is assumed to be the Higgs boson, and M_p is the Planck energy scale. The parameters ξ and ξ_h represent two nonminimal couplings. In the limit that $\sigma \ll M_p$, the potential can be expanded as

$$V(\sigma)=\frac{1}{4}\left(\lambda-\frac{1}{9}\xi_h\xi^2+\frac{1}{6}\xi_h^2\xi^2\right)\sigma^4-\frac{1}{2}\xi_h\xi^2M_p^2\sigma^2+\cdots, \tag{26}$$

which takes the form of Higgs potential of the SM. In order to comply with the value of the Higgs mass and EW VEV, the parameters $\xi\sqrt{\xi_h}\sim 3.5\times 10^{-17}$ and $\lambda\sim\lambda_{\rm SM}$ are chosen as shown in the second row of Table V.

In the Ref. [60], in terms of scale transformation, by introducing the spurion field into the low-energy effective theory, the general dilaton potential can be of the form

$$V(\chi)=\chi^4\sum_{n=0}^{\infty}c_n(\Delta_{\mathcal{O}})\left(\frac{\chi}{f}\right)^{n(\Delta_{\mathcal{O}}-4)}, \tag{27}$$

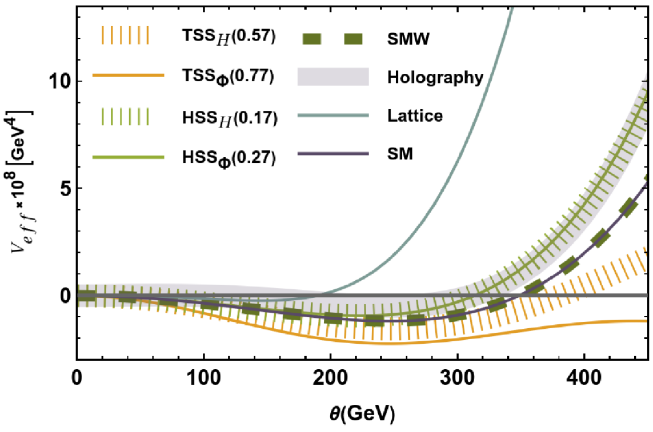


FIG. 6. The shape of Higgs potentials are demonstrated.

TABLE V. The typical orders of parameters in SMW [12] to accommodate experimental data are provided.

Framework	ξ_h	ξ
Particle Physics (set A)	$\xi\sqrt{\xi_h}\sim 3.5\times 10^{-17}$ To fix the mass of H_{125}	
Cosmology (set B)	10^{-3}–10^{-2} Inflation	10^{-9} CMB

where $\chi=f+\bar{\chi}$, with $\bar{\chi}(x)$ representing the dilaton field, f being the VEV of χ, and $\Delta_{\mathcal{O}}$ denoting the dimension of the operator $\mathcal{O}$ that breaks conformal symmetry. And the coefficients c_n depend on the dynamics of the underlying conformal field theory. In the limit $\Delta_{\mathcal{O}}\to 4$, the Coleman-Weinberg correction to the potential can be of the form

$$V(\chi)=\frac{1}{16}\frac{m^2}{f^2}\chi^4\left[4\ln\frac{\chi}{f}-1\right]+\mathcal{O}(|\Delta_{\mathcal{O}}-4|^2). \tag{28}$$

It includes the SSB scale f, which is set as $f=v_{\rm SM}$ and $m\sim m_{\rm H_{125}}/\sqrt{2}$ GeV in order to compare and contrast with other potentials in Fig. 6.

In Refs. [61,62], in order to explore the dynamic of conformal symmetry breaking, an effective field theory of dilaton field is constructed by using lattice data. The effective potential of dilaton field can be cast into a form as given below

$$V(\chi)=\frac{m_d^2\chi^4}{4(4-\Delta_{\mathcal{O}})f_d^2}\left[1-\frac{4}{\Delta_{\mathcal{O}}}\left(\frac{f_d}{\chi}\right)^{4-\Delta_{\mathcal{O}}}\right]-\frac{N_f m_\pi^2 f_\pi^2}{2}\left(\frac{\chi}{f_d}\right)^y. \tag{29}$$

The final term in the potential arises from light quark contributions, where m_π and f_π represent the mass and decay constant of the pion fields, respectively. This term is essential for the lattice method and explicitly breaks scale symmetry through the tunable mass m_π. The soft theorem suggests that $\Delta_{\mathcal{O}}\to 2$ at the infrared fixed point [63]. Compared with Eq. (28), these represent two extreme cases of conformal symmetry breaking caused by either a gluon condensate $\Delta_{\mathcal{O}}=\Delta_{G2}=4$ or a fermion condensate $\Delta_{\mathcal{O}}=\Delta_{\bar{f}f}=2$. Lattice data yield a more comprehensive result of $\Delta_{\mathcal{O}}=3.5$ with $y=2.06\pm 0.05$ by using SU(3) YM theory with $N_f=8$ Dirac fermions in the fundamental representation. The parameters m_d and m_π are fixed to determine the mass of $\rm H_{125}$ by the definitions. All parameters for Fig. 6 are presented in the Table 1 of [61].

It is noteworthy that potentials given in Eqs. (28) and (29) can also be introduced to explicitly break the local conformal symmetry of the Lagrangian in Eq. (2) as well, which belong to the second method. Here these two

TABLE VI. Higgs potentials in a few typical models are provided and compared.

Model	Potential	VEV (GeV)	Parameters
TSS	Eq. (15)	246.3	s = 0.57, $\kappa_V = 1$
		246.3	s = 0.77, $\kappa_V = 1$
HSS	Eq. (19)	221.64	s = 0.17, $\kappa_V = 1.112$
		223.88	s = 0.27, $\kappa_V = 1.112$
SMW [12]	Eq. (26)	246.3	$\xi\sqrt{\xi_h} \sim 3.5 \times 10^{-17}$
			$\lambda \sim \lambda_{\rm SM}$
Holography [45,60]	Eq. (28)	246.3	$\Delta_{\mathcal{O}} \to 4$
			$f = v_{\rm SM}$
			$m = m_{\rm H_{125}}/\sqrt{2}$
Lattice [61,62]	Eq. (29)	144.47	$N_f = 8$
			$\Delta = 3.5$
			$y = 2.06 \pm 0.05$
			$m_d = 125$ GeV
			$m_\pi = 0.2$ MeV
SM	Eq. (1)	246.3	$\lambda_{\rm SM} = 0.13$

potentials serve as the template potentials to describe the dilaton-dominant cases.

After choosing some parameters as given in Table VI, we plot the shape of these Higgs potentials which are shown in Fig. 6. For the scenarios we discuses above, we thoroughly demonstrate each possibility. The orange curves represent two TSS cases: the dotted curve is the doublet dominance with $s = 0.57$ and the thick curve is dilaton dominance with $s = 0.77$. Meanwhile, there are two HSS cases one for the doublet dominance with $s = 0.17$ and the other one for dilaton dominance with $s = 0.27$ which are shown in blue curves. The potential of SMW model is plotted by a dashed curve while the potential determined from lattice calculation is drawn by using a darker cyan curve. A shallow purple curve is to represent the Higgs potential in the holographic framework, incorporating the Coleman-Weinberg correction. The purple curve is for the Higgs potential of the SM.

An obvious feature is that these scalar potentials can trigger spontaneous EW symmetry breaking successfully after the conformal symmetry breaking and can accommodate Higgs data, the correspondent mass of H_{125} demonstrated in the third column of Table VI which is fixed at 125.11 GeV. There are a few comments in order.

(i) Although the VEV of HSS is different from that of the SM, it is consistent with experimental errors.

(ii) The holographic potential closely resembles the HSS type potential, although the VEVs differ between the two distinct models. The underlying reason may stem from the mathematical framework in which the scale transformation is described by a hyperbolic function. Further aspects of the physical relationship warrant additional investigation.

(iii) One special exception is the lattice type, where the VEV is 144.47 GeV. The gap between theoretical and experimental VEV is large. Since the parameters m_π or f_π are adjustable, the VEV can be accurately determined, albeit with a corresponding adjustment in the associated mass term.

(iv) Two key points should be highlighted, for which the potential of TSS-dilaton in Fig. 6 starts to drop down after $\theta > 450$ GeV. First, because the TSS potential depicted is based on a VEV of 246.3 GeV, the expansion is less reliable for $\theta > 450$ GeV. Second, the full potential exhibits oscillatory behavior, which can be attributed to the trigonometric function within Eq. (15).

(v) A remarkable character of our model is that the potentials of HSS are exponentially dependent upon h while those of TSS are periodic, which might have some different effects during phase transitions.

VI. DISCUSSIONS AND CONCLUSIONS

In this paper, we investigate the scalar sector of a dilaton model with the local gauge conformal symmetry $D(1)$. In the model, two scenarios, TSS and HSS, are identified due to uncertainties in the linearization from quadratic gravity to general relativity. Furthermore, after taking into account both theoretical requirements and experimental bounds, we find the allowed parameter space of the model. Our findings support the thought that the scalar boson found at the LHC with a mass 125 GeV could be dilaton dominance and it can be further addressed by the HL-LHC. Apart from that, we also give predictions of the four-point Higgs self-coupling for TSS and also HSS showing that both of them have weaker interactions than SM prediction. In the end, we compare the potential in our model with other models showing that it can give the same Higgs mass for H_{125} based on different VEV and the distinct sharpness of TSS and HSS compared to the SM imply the thorough analysis of our model.

In this work, we consider a simple dilaton model and we can extend our results to other BSM models. In our analysis, we observe that the Yukawa couplings can constrain the model parameters strongly, i.e., most of the parameter space of dilaton dominance can be excluded by k_f measurements.

The results shown in Fig. 3 are obviously model dependent, where we assume that the dilaton field does not couple to fermions. Such results might be changed drastically if Yukawa couplings of the dilaton (singlet) field and fermions are assumed, like the couplings of radion and fermions in the Randall-Sundrum (RS) model [24,64] and the couplings of the singlet field with vectorlike fermions in the top quark seesaw mechanism [27,65]. In these cases, larger parameter space of dilaton dominance might still be allowed by the LHC Higgs data. For example, the dilaton-dominant region for $s > 0.6$ in the TSS scenario might still be allowed if the couplings of dilaton and fermion fields are assumed. The couplings of the dilaton (singlet) field with fermions opens more potential theoretical interpretation of the observed 125 GeV Higgs boson H_{125} as originating from the dilaton (singlet) scalar Φ. At the same time, such couplings also offer theoretical potential to address more fundamental issues related to the neutrino masses and mixings, as shown in [31].

The Weyl vector ω_μ, which becomes massive after scale-symmetry breaking, is naturally predicted to be a Higgs-portal dark-matter candidate [30,66,67]. In particular, it decouples from Higgs interactions at $\chi = 0$ within the TSS framework. The gravitational waves might be produced by the phase transition accompanying with the conformal symmetry breaking [68]. The model itself can be applied to interpret precision cosmology experiments, as demonstrated in [69,70]. Therefore, within this simple dilaton model, it is possible to shed light on the connection between particle physics and gravity.

However, the existence of a set of parameters that can accommodate both cosmological and particle physics data deserves a careful study. At the current stage, there is an obvious tension in the SMW [12,70], where two sets of parameters for ξ_h and ξ in Eq. (26) must be introduced in order to accommodate cosmological data (set B) and particle physics data (set A) as given in Table V. The set A of parameters for EW spontaneous symmetry breaking used in Fig. 6 is fixed at $\xi\sqrt{\xi_h} \sim 3.5 \times 10^{-17}$ to produce the mass of H_{125}, which is significantly different from the cosmological set, where the set B of parameters requires that $\xi_h \sim 10^{-3}$–10^{-2} and $\xi \sim 10^{-9}$ in order to accommodate inflation and CMB data. In term of $\xi\sqrt{\xi_h}$, the difference between these two sets of parameter can reach up to about 6–7 orders of magnitude, while in terms of the scalar masses, the difference is 10 orders of magnitude. Such a tension deserves our further study.

The current work focuses on tree-level effects and collider phenomenological analysis, which remain meaningful at this stage. While in order to address the tension mentioned above, it might require us to take into account inflation models and quantum corrections [69,71]. The solutions of this tension may shed light on the Higgs-related questions from the perspective of gravity and to investigate new physics using both collider and cosmology data.

Our model can give an explanation to the gravitational constant G and the cosmological constant Λ, as in scalar-tensor theory [49] after assuming $f \sim \Lambda_{\rm Pl}$, because the model is constructed from a Weyl-gauge theory of gravity. However, the large hierarchy between the scales f and $f_{\rm EW}$ demands unnatural large parameters $\chi_{H,D}$ as seeing from Eqs. (16) and (20). So, we would like to assume the scale f is lower than $\Lambda_{\rm Pl}$. Since we focus on the phenomenological analysis of the model in light of LHC measurements, the scale $f_{\rm EW}$ is fixed while the scale symmetry breaking scale while the scale f remains undetermined.

The last but not the least, it is necessary to address the issue of the radiative stability of the lighter scales in our model. As presented above, our model involves three fundamental physics scales, i.e., Planck energy scale $\Lambda_{\rm Pl}$, conformal symmetry breaking scale f, and the electroweak breaking scale $f_{\rm EW}$. It is natural to ask what mechanism can prevent the lighter scale, like $f_{\rm EW}$, from being driven toward the heavier one, like f, by radiative corrections? Moreover, if the scale f is distinct from the scale $\Lambda_{\rm Pl}$, what prevents it from being pushed up to $\Lambda_{\rm Pl}$ by quantum effects? In other words, when the relation $\Lambda_{\rm Pl} \gg f \gg f_{\rm EW}$ is assumed, this issue include two-fold aspects, the first aspect is why f cannot be driven up to $\Lambda_{\rm Pl}$, and the second aspect is why $f_{\rm EW}$ cannot be driven up to f by quantum corrections.

In order to address this issue, it is necessary to clarify scales in our model. At its face values, there are two sets of scales. The first set, (f_H, f_D), corresponds to the VEVs of the doublet scalar ϕ and dilaton Φ in the interaction basis. And the second set, $(f, f_{\rm EW})$, corresponds to the physical scales associated with scale symmetry breaking and electroweak symmetry breaking. Due to the relation described in Eq. (7), the first set of parameters determines the second set of the parameter after the symmetries breaking.

It is noteworthy that our model offers a dynamic way to generate the mass term of the Higgs sector of the SM. For example, when the conformal symmetry is broken, saying Φ develops a vacuum f_D for instance, the mass term of the SM Higgs given in Eq. (1) can be generated, which reads

$$\mu^2 = -\frac{\alpha}{2} f_D^2 \tag{30}$$

The sign of α must be negative in order to have a nonvanishing f_H. Since f is the physical scale for the gauged scale symmetry breaking and, as shown in Eqs. (16) and (20), $f_{\rm EW}$ is proportional to f by the following relation

$$f_{\rm EW} \approx f \sqrt{\frac{-\alpha + \frac{\rho\chi_H^2}{3\chi_D^2}}{2\chi_D^2\left(\lambda + \frac{\rho\chi_H^4}{6\chi_D^4} - \frac{\alpha\chi_H^2}{\chi_D^2}\right)}} \tag{31}$$

if $\frac{\chi_H}{f}U_t$ is a small number in the TSS, or by the relation

$$f_{\rm EW} \approx f\sqrt{\frac{-\alpha-\frac{\rho}{3}\frac{\chi_H^2}{\chi_D^2}}{2\chi_D^2\left(\lambda+\alpha\frac{\chi_H^2}{\chi_D^2}+\frac{\rho}{6}\frac{\chi_H^4}{\chi_D^4}\right)}} \tag{32}$$

if $\frac{\chi_H}{f}U_h$ is a small number in the HSS. It is observed that these two physical scales, f and $f_{\rm EW}$, are connected with each other in the model.

On the first aspect of the issue, if $\Lambda_{\rm Pl} \gg f$, whether the radiative corrections can drive f up to $\Lambda_{\rm Pl}$? The answer is no. For example, in composite Higgs models, the scale f arises from gluon condensates [72] or fermion condensates [62,63,73]. If the scale f is much smaller than $\Lambda_{\rm Pl}$, above the scale f, the conformal symmetry can work and guarantee f is only a low energy scale and can keep f being smaller than $\Lambda_{\rm Pl}$. Supposing the dilaton field is a low energy degree of freedom from gluon condensates, like in the setup of Ref. [72]. Above the scale f, the low energy effective theory of dilaton field turns into a pure Yang-Mills theory which respects the conformal symmetry exactly, where the scale f is a low energy scale and might be directly related with the dimensional transmutation of strong Yang-Mills dynamics.

The second aspect of the issue is more subtle. If two physical scales f and $f_{\rm EW}$ are close to each other, saying $f \sim f_{\rm EW}$, there is no need to worry about the radiative stability of the model.

While for the case $f \gg f_{\rm EW}$ (saying $f = 10^{3-15} f_{\rm EW}$), we have to face with the issue of radiative stability for the lighter scale or our model will suffer the little/big hierarchy problem. Since below f there is no remaining conformal symmetry to protect the mass term μ^2 from getting a large quantum correction, it is expected that the quantum correction of μ^2 should be $\mu^2 + \delta\mu^2 \propto f_{\rm EW}^2 + Cf^2$ (where C is related to model parameters), just like the quadratic divergence of Higgs mass term in the SM.

The issue of radiative stability of $f_{\rm EW}$ can be investigated in the holographic RS model. In RS model [74], the effective scales $f \sim \Lambda_{\rm Pl}$ and $f_{\rm EW}$, arise from UV and IR branes, respectively. A bulk scalar, called as the radion, is introduced to stabilize the warped geometry of the extra dimension [75]. The hierarchy problem is translated into the warp factor between the UV and IR branes and is controlled by the radion. Within the holographic framework, the duality between the radion and the dilaton introduces a scale symmetry that can prevent the scale $f_{\rm EW}$ from being pushed to $\Lambda_{\rm Pl}$ by quantum corrections [76] as long as the scaling dimension $\Delta_{\mathcal{O}}$ approaches the canonical dimension $d_{\mathcal{O}}$ [45], which gives rise to the Coleman-Weinberg correction [60]. Other plausible mechanisms in literature [77–79], such as an approximate shift symmetry for the light scalar [80], compositeness [81], or near-conformal dynamics operative below f [82,83], could protect the lighter scale without qualitatively altering the phenomenological studied in this work.

Therefore, we can conclude that an exact or approximate gauged scale symmetry above the scale f can keeps the scale f to be stable if $\Lambda_{\rm Pl} \gg f$, while additional dynamics might be needed if $f \gg f_{\rm EW}$ in order to keep the lower scale $f_{\rm EW}$ stable. In our phenomenological analysis, we have fixed $f_{\rm EW}$ and have left f as a free parameter. Thus our results is independent of the actual stabilizing mechanism for the lower scale $f_{\rm EW}$.

ACKNOWLEDGMENTS

We thank Sichun Sun, Yong Tang, and Tianrui Che for useful discussions. This work is supported by the Natural Science Foundation of China under the Grants No. 11875260 and No. 12275143.

DATA AVAILABILITY

No data were created or analyzed in this study.

[1] Georges Aad *et al.* (ATLAS Collaboration), Observation of a new particle in the search for the standard model Higgs boson with the ATLAS detector at the LHC, Phys. Lett. B **716**, 1 (2012).
[2] Serguei Chatrchyan *et al.* (CMS Collaboration), Observation of a new boson at a mass of 125 GeV with the CMS experiment at the LHC, Phys. Lett. B **716**, 30 (2012).
[3] B. P. Abbott *et al.* (LIGO Scientific and Virgo Collaborations), Observation of gravitational waves from a binary black hole merger, Phys. Rev. Lett. **116**, 061102 (2016).
[4] K. S. Stelle, Renormalization of higher derivative quantum gravity, Phys. Rev. D **16**, 953 (1977).
[5] Petr Horava, Quantum gravity at a Lifshitz point, Phys. Rev. D **79**, 084008 (2009).
[6] Leonardo Modesto, Super-renormalizable quantum gravity, Phys. Rev. D **86**, 044005 (2012).
[7] Kenji Hayashi, Masahiro Kasuya, and Takeshi Shirafuji, Elementary particles and Weyl's gauge field, Prog. Theor. Phys. **59**, 681 (1978).
[8] K. Hayashi and T. Kugo, Remarks on Weyl's gauge field, Prog. Theor. Phys. **61**, 334 (1979).
[9] D. M. Ghilencea and Hyun Min Lee, Weyl gauge symmetry and its spontaneous breaking in the standard model and inflation, Phys. Rev. D **99**, 115007 (2019).

[10] D. M. Ghilencea, Spontaneous breaking of Weyl quadratic gravity to einstein action and Higgs potential, J. High Energy Phys. 03 (2019) 049.
[11] D. M. Ghilencea, Stueckelberg breaking of Weyl conformal geometry and applications to gravity, Phys. Rev. D **101**, 045010 (2020).
[12] D. M. Ghilencea, Standard model in Weyl conformal geometry, Eur. Phys. J. C **82**, 23 (2022).
[13] D. M. Ghilencea, Nonmetric geometry as the origin of mass in gauge theories of scale invariance, Eur. Phys. J. C **83**, 176 (2023).
[14] D. M. Ghilencea and C. T. Hill, Standard model in conformal geometry: Local vs gauged scale invariance, Ann. Phys. (Amsterdam) **460**, 169562 (2024).
[15] H. Weyl, Gravitation and electricity, Sitzungsber. Preuss. Akad. Wiss. Berlin (Math. Phys.) **1918**, 465 (1918).
[16] Paul A. M. Dirac, Long range forces and broken symmetries, Proc. R. Soc. A **333**, 403 (1973).
[17] L. O'Raifeartaigh, *The Dawning of Gauge Theory* (Princeton University Press, Princeton, NJ, USA, 1997).
[18] Yasunori Fujii, Origin of the gravitational constant and particle masses in scale invariant scalar—tensor theory, Phys. Rev. D **26**, 2580 (1982).
[19] W. Drechsler and H. Tann, Broken Weyl invariance and the origin of mass, Found. Phys. **29**, 1023 (1999).
[20] Ali H. Chamseddine, Alain Connes, and Matilde Marcolli, Gravity and the standard model with neutrino mixing, Adv. Theor. Math. Phys. **11**, 991 (2007).
[21] Th. Kaluza, Zum Unitätsproblem der Physik, Sitzungsber. Preuss. Akad. Wiss. Berlin (Math. Phys.) **1921**, 966 (1921).
[22] Oskar Klein, Quantum theory and five-dimensional theory of relativity. (In German and English), Z. Phys. **37**, 895 (1926).
[23] K. Becker, M. Becker, and J. H. Schwarz, *String Theory and M-Theory: A Modern Introduction* (Cambridge University Press, Cambridge, England, 2006).
[24] Vernon Barger, Muneyuki Ishida, and Wai-Yee Keung, Differentiating the Higgs boson from the dilaton and radion at hadron colliders, Phys. Rev. Lett. **108**, 101802 (2012).
[25] Shinya Matsuzaki and Koichi Yamawaki, Discovering the 125 GeV techni-dilaton at the LHC, Phys. Rev. D **86**, 035025 (2012).
[26] Brando Bellazzini, Csaba Csáki, Jay Hubisz, Javi Serra, and John Terning, A Higgs-like dilaton, Eur. Phys. J. C **73**, 2333 (2013).
[27] Tomohiro Abe, Ryuichiro Kitano, Yasufumi Konishi, Kinya Oda, Joe Sato, and Shohei Sugiyama, Minimal dilaton model, Phys. Rev. D **86**, 115016 (2012).
[28] Moshe Flato and Ryszard Raczka, A possible gravitational origin of Higgs field in the standard model, Phys. Lett. B **208**, 110 (1988).
[29] J. J. van der Bij, Can gravity make the Higgs particle decouple?, Acta Phys. Pol. B **25**, 827 (1994).
[30] Hung Cheng, Possible existence of Weyl's vector meson, Phys. Rev. Lett. **61**, 2182 (1988).
[31] Hitoshi Nishino and Subhash Rajpoot, Broken scale invariance in the standard model, arXiv:hep-th/0403039.
[32] Hitoshi Nishino and Subhash Rajpoot, Implication of compensator field and local scale invariance in the standard model, Phys. Rev. D **79**, 125025 (2009).
[33] Marco de Cesare, John W. Moffat, and Mairi Sakellariadou, Local conformal symmetry in non-Riemannian geometry and the origin of physical scales, Eur. Phys. J. C **77**, 605 (2017).
[34] Friedrich W. Hehl, J. Dermott McCrea, Eckehard W. Mielke, and Yuval Ne'eman, Metric-affine gauge theory of gravity: Field equations, Noether identities, world spinors, and breaking of dilation invariance, Phys. Rep. **258**, 1 (1995).
[35] A. Trautman, The geometry of gauge fields. (Talk), Czech. J. Phys. B **29**, 107 (1979).
[36] Georges Aad *et al.* (ATLAS Collaboration), A detailed map of Higgs boson interactions by the ATLAS experiment ten years after the discovery, Nature (London) **607**, 52 (2022); **612**, E24 (2022).
[37] Giuseppe Degrassi, Pier Paolo Giardino, Fabio Maltoni, and Davide Pagani, Probing the Higgs self coupling via single Higgs production at the LHC, J. High Energy Phys. 12 (2016) 080.
[38] Kenneth Lane, The composite Higgs signal at the next big collider, in Snowmass 2021 (2022), arXiv:2203.03710.
[39] Thomas Steingasser and David I. Kaiser, Higgs potential criticality beyond the standard model, Phys. Rev. D **108**, 095035 (2023).
[40] Georges Aad *et al.* (ATLAS Collaboration), Combination of searches for Higgs boson pair production in pp collisions at $\sqrt{s} = 13$ TeV with the ATLAS detector, Phys. Rev. Lett. **133**, 101801 (2024).
[41] Report on the physics at the HL-LHC and perspectives for the HE-LHC (2019), 10.23731/CYRM-2019-007.
[42] Shiing-Shen Chern, A simple intrinsic proof of the Gauss-Bonnet formula for closed Riemannian manifolds, Ann. Math. **45**, 747 (1944).
[43] Shiing shen Chern, On the curvatura integra in a Riemannian manifold, Ann. Math. **46**, 674 (1945).
[44] Sidney R. Coleman and Erick J. Weinberg, Radiative corrections as the origin of spontaneous symmetry breaking, Phys. Rev. D **7**, 1888 (1973).
[45] R. Rattazzi and A. Zaffaroni, Comments on the holographic picture of the Randall-Sundrum model, J. High Energy Phys. 04 (2001) 021.
[46] Henri Ruegg and Marti Ruiz-Altaba, The Stueckelberg field, Int. J. Mod. Phys. A **19**, 3265 (2004).
[47] Salvatore Capozziello and Mariafelicia De Laurentis, Extended theories of gravity, Phys. Rep. **509**, 167 (2011).
[48] Curtis G. Callan, Jr., Sidney R. Coleman, and Roman Jackiw, A new improved energy—momentum tensor, Ann. Phys. (N.Y.) **59**, 42 (1970).
[49] Valerio Faraoni, *Cosmology in Scalar-Tensor Gravity*, Fundamental Theories of Physics Vol. 139 (Kluwer Academic Publishers, Dordrecht; Boston, 2004).
[50] Georges Aad *et al.* (ATLAS Collaboration), Measurement of the W-boson mass and width with the ATLAS detector using proton–proton collisions at $\sqrt{s} = 7$ TeV, Eur. Phys. J. C **84**, 1309 (2024).
[51] Georges Aad *et al.* (ATLAS Collaboration), Measurement of the Higgs boson mass with $H \to \gamma\gamma$ decays in 140 fb^{-1} of $\sqrt{s} = 13$ TeV pp collisions with the ATLAS detector, Phys. Lett. B **847**, 138315 (2023).

[52] Georges Aad *et al.* (ATLAS Collaboration), A detailed map of Higgs boson interactions by the ATLAS experiment ten years after the discovery, Nature (London) **607**, 52 (2022); **612**, E24 (2022).
[53] Combined measurements of Higgs boson production and decay at $\sqrt{s} = 13$ TeV using up to 140 fb^{-1} of data collected by the ATLAS Experiment (2025), https://cds.cern.ch/record/2937634.
[54] Georges Aad *et al.* (ATLAS Collaboration), Measurement of the W-boson mass and width with the ATLAS detector using proton-proton collisions at $\sqrt{s} = 7$ TeV, Eur. Phys. J. C **84**, 1309 (2024).
[55] Georges Aad *et al.* (ATLAS Collaboration), Characterising the Higgs boson with ATLAS data from run 2 of the LHC, Phys. Rep. **1116**, 4 (2025).
[56] Abdelhak Djouadi, The anatomy of electro-weak symmetry breaking. I: The Higgs boson in the standard model, Phys. Rep. **457**, 1 (2008).
[57] Chien-Yi Chen, Qi-Shu Yan, Xiaoran Zhao, Yi-Ming Zhong, and Zhijie Zhao, Probing triple-Higgs productions via 4b2γ decay channel at a 100 TeV hadron collider, Phys. Rev. D **93**, 013007 (2016).
[58] Wolfgang Kilian, Sichun Sun, Qi-Shu Yan, Xiaoran Zhao, and Zhijie Zhao, New physics in multi-Higgs boson final states, J. High Energy Phys. 06 (2017) 145.
[59] Wolfgang Kilian, Sichun Sun, Qi-Shu Yan, Xiaoran Zhao, and Zhijie Zhao, Multi-Higgs boson production and unitarity in vector-boson fusion at future hadron colliders, Phys. Rev. D **101**, 076012 (2020).
[60] Walter D. Goldberger, Benjamin Grinstein, and Witold Skiba, Distinguishing the Higgs boson from the dilaton at the large hadron collider, Phys. Rev. Lett. **100**, 111802 (2008).
[61] Thomas Appelquist, James Ingoldby, and Maurizio Piai, Dilaton potential and lattice data, Phys. Rev. D **101**, 075025 (2020).
[62] Thomas Appelquist, James Ingoldby, and Maurizio Piai, Dilaton effective field theory, Universe **9**, 10 (2023).
[63] Roman Zwicky, QCD with an infrared fixed point and a dilaton, Phys. Rev. D **110**, 014048 (2024).
[64] Csaba Csaki, Jay Hubisz, and Seung J. Lee, Radion phenomenology in realistic warped space models, Phys. Rev. D **76**, 125015 (2007).
[65] Hong-Jian He, Christopher T. Hill, and Tim M. P. Tait, Top quark seesaw model, vacuum structure, and electroweak precision constraints, Phys. Rev. D **65**, 055006 (2002).
[66] Chao-guang Huang, Dan-di Wu, and Han-qing Zheng, Cosmological constraints to Weyl's vector meson, Commun. Theor. Phys. **14**, 373 (1990).
[67] Yong Tang and Yue-Liang Wu, Weyl symmetry inspired inflation and dark matter, Phys. Lett. B **803**, 135320 (2020).
[68] Amine Ahriche, Shinya Kanemura, and Masanori Tanaka, Gravitational waves from phase transitions in scale invariant models, J. High Energy Phys. 01 (2024) 201.
[69] Yong Tang and Yue-Liang Wu, Inflation in gauge theory of gravity with local scaling symmetry and quantum induced symmetry breaking, Phys. Lett. B **784**, 163 (2018).
[70] D. M. Ghilencea, Gauging scale symmetry and inflation: Weyl versus Palatini gravity, Eur. Phys. J. C **81**, 510 (2021).
[71] John F. Donoghue and Gabriel Menezes, Inducing the Einstein action in QCD-like theories, Phys. Rev. D **97**, 056022 (2018).
[72] A. A. Migdal and M. A. Shifman, Dilaton effective Lagrangian in gluodynamics, Phys. Lett. B **114**, 445 (1982).
[73] Steven Weinberg, Implications of dynamical symmetry breaking, Phys. Rev. D **13**, 974 (1976); **19**, 1277(A) (1979).
[74] Lisa Randall and Raman Sundrum, A large mass hierarchy from a small extra dimension, Phys. Rev. Lett. **83**, 3370 (1999).
[75] Walter D. Goldberger and Mark B. Wise, Modulus stabilization with bulk fields, Phys. Rev. Lett. **83**, 4922 (1999).
[76] Paul H. Frampton and Cumrun Vafa, Conformal approach to particle phenomenology, arXiv:hep-th/9903226.
[77] Csaba Csaki, Christophe Grojean, and John Terning, Alternatives to an elementary Higgs, Rev. Mod. Phys. **88**, 045001 (2016).
[78] Csaba Csáki, Salvator Lombardo, and Ofri Telem, TASI lectures on non-supersymmetric BSM models, in *Anticipating the Next Discoveries in Particle Physics* (World Scientific Publishing, Singapore, 2018), pp. 501–570.
[79] Csaba Csáki, Salvator Lombardo, and Ofri Telem, Non-supersymmetric BSM models, Eur. Phys. J. Special Topics **231**, 1229 (2022).
[80] Peter W. Graham, David E. Kaplan, and Surjeet Rajendran, Cosmological relaxation of the electroweak scale, Phys. Rev. Lett. **115**, 221801 (2015).
[81] Gabriele Ferretti, Underlying gauge-fermion models of compositeness, Eur. Phys. J. Special Topics **231**, 1265 (2022).
[82] O. Catà, R. J. Crewther, and Lewis C. Tunstall, Crawling technicolor, Phys. Rev. D **100**, 095007 (2019).
[83] R. J. Crewther, Genuine dilatons in gauge theories, Universe **6**, 96 (2020).